Microscopic analysis of the influence of strain and band-gap offsets on noise characteristics in $Si_{1-x}Ge_x$/Si heterojunctions

M. J. Martín Martinez,[a] D. Pardo, and J. E. Velázquez
Departamento de Fisica Aplicada, Universidad de Salamanca, Plaza de la Merced s/n, 37008 Salamanca, Spain

(Received 31 March 1998; accepted for publication 25 July 1998)

A detailed study under forward-bias conditions of the physical origin of high frequency noise in p^+(Si)-n ($Si_{1-x}Ge_x$) heterojunctions using ensemble Monte Carlo simulation is reported. Based on the internal magnitudes, we determine how the strained SiGe layer induces different features in the perpendicular transport of a heterojunction as compared with that of a silicon p^+n homojunction. The main part of this study focuses on a comparative microscopic analysis of current fluctuations in homojunction and heterojunctions over a wide range of frequencies. A method based on considering a spatial analysis of noise to isolate the contributions of both types of carrier on the Si and $Si_{1-x}Ge_x$ epilayers of the devices is described. The role of electrons and holes in the different regions of the devices and the combined effects of the band discontinuities and strain on noise characteristics in $Si_{1-x}Ge_x$/Si bipolar heterojunctions is discussed. © *1998 American Institute of Physics.* [S0021-8979(98)01521-7]

I. INTRODUCTION

During the past few years, structures based on the pseudomorphic $Si_{1-x}Ge_x$ strained layer on Si systems have played an important role in the improvement of existing devices and the development of new ones. With this layer, additional degrees of freedom can be introduced into the design of the device as a result of band-gap engineering.[1] Specifically, the heterostructure bipolar transistor (HBT) allows a dramatic increase in the base doping without degrading the current gain and hence a reduction in both base resistance and base width. This is crucial for enhancing the speed and minimizing the microwave noise of bipolar circuits.[2] The analysis of current fluctuations and the different phenomena that originate microwave noise is a powerful tool for characterizing this technology and for studying the degradation of SiGe HBTs performance. Important types of noise that affect current flow are $1/f$, shot, generation–recombination and thermal noise.[3] Some of them, such as $1/f$ and generation–recombination noise, can be restricted by the choice of an optimum device design and fabrication process. However, thermal noise is generated by mechanisms that are intrinsic to the dynamic nature of carrier transport, and therefore presents a lower noise limit in all semiconductor devices. To evaluate this limit, and optimize the signal–to–noise ratio it is necessary to gain insight into processes that give rise to current fluctuations.

These microscopic noise sources have been extensively studied in semiconductor materials and unipolar devices[4–8] considering band structure, lattice phonons and charged impurity scattering, space charge effects, etc. However, study of noise phenomena occurring in a HBT is a complex problem involving many physical additional mechanisms responsible for different noise sources (generation–recombination mechanisms, fluctuations in barrier height, quantum transport at the heterojunction, energy levels quantization, carrier mass change between both sides of the junction, etc.). As an initial step for this purpose, noise in silicon bipolar homojunctions has been previously studied to determine precisely the origin of the current fluctuations due to the classic transport of diffusive type.[9] Furthermore, the physical interpretation of the total current fluctuations in terms of the electron, hole, and crossed (electron-hole and hole-electron) fluctuations was performed. Recently, preliminary qualitative results evaluating the effect of strained SiGe layers on current noise in bipolar devices have been presented,[10,11] but the physical origin of high frequency noise phenomena in SiGe/Si heterojunctions has still not been fully explained. Prior to an accurate study of a complex heterostructure, in this article we present a one-dimensional analysis of $Si_{1-x}Ge_x$/Si bipolar heterojunctions for values of the Ge molar fraction x equal to 0 and 0.3. An attempt is made to investigate the role of both types of carrier in different regions of the devices and to determine the combined effects of the germanium profile, band discontinuities, and strain on both perpendicular transport and current fluctuations in the microwave frequency range. Owing to the aims of the work and in view of the submicrometer dimensions of the structures (such that carrier transport is nonstationary), the presence of strain effects, and the many transport phenomena involved, the best technique for performing a detailed study of transport is by means of an ensemble Monte Carlo (EMC) method.[12]

In the following section the features of our one-dimensional bipolar EMC simulator are discussed specifically in relation to the transport properties of a strained SiGe layer grown on a Si substrate. In Sec. III a description of the simulated structures is given. Section IV focuses on the stationary carrier transport results. In Sec. V the theory behind our bipolar noise calculations is described. A comparative

[a]Electronic mail: mjesus@rs6000.usal.es

study of the noise characteristic is offered in Sec. VI. This includes a discussion of the low and high frequency behavior of the spectral density of total current fluctuations. Finally, the conclusions of this work are summarized in Sec. VII.

II. MATERIAL TRANSPORT PROPERTIES OF $Si_{1-x}Ge_x$ GROWN ON [001] SI

For electron transport in Si, our EMC simulator considers anisotropic and nonparabolic X and L valleys of the conduction band (CB).[13] The Δ conduction band minimum in Si has sixfold spatial degeneracy. The character of the CB of SiGe remains Si-like up to a Ge molar fraction of 0.85.[14] The SiGe alloy grown on the [001] Si substrate is under biaxial compressive strain. This splits the band into: (a) a fourfold state ([100] and [010] valleys) whose valleys constitute the minimum of the CB. These valleys are designated as X transverse valleys or $X_\perp$. (b) A twofold state ([001] valleys) whose valleys are designated as longitudinal X valleys or $X_\parallel$. This lifting of the degeneracy on X valleys induces strong anisotropy in electron carrier mobility. Theoretical investigations have suggested that the Δ conduction band mass parameters remain unaffected up to 85% Ge and that they are rather insensitive to strain.[15] We thus assume that the effective mass tensor is that of silicon.[16]

Both heavy hole (HH) and light hole (LH) subbands of the valence band (VB) are included in our p-type Si model.[17] The hole transport in lattice-matched $Si_{1-x}Ge_x$ layers grown on a Si substrate and subject to a biaxial stress, in the [001] direction, undergoes different effects.[18] One of the most important of these is the reduction in the gap, mainly originated by an upward shift of the HH subband of the usual degenerate HH and LH subbands in the Γ point.[19]

Knowledge of strained band gaps and strain dependent band offsets is critical for obtaining high performance SiGe HBTs. The effect of strain on the band structure is expressed via deformation potentials. Band offsets are also intimately coupled with the strain effects. In handling the structure of strained SiGe alloys and choosing the deformation potentials for Si and Ge used in the simulation, we followed the work of Van de Walle and Martin.[17,20] In order to simulate the alloy, it is a good approximation to assume that for low Ge percentages the deformation potentials of VB and CB, the HH and LH effective masses and the band offsets between the valence bands are given by linear interpolation. Thus, the latter parameters show very strong agreement with the experimental optical and electrical calculations.[21,22] The parameters for bulk Si and Ge employed in our simulation (masses, lattice and elastic constants, and sound velocities) can be found in Ref. 23.

The scattering mechanisms considered for electrons and holes are similar to those reported for Si.[9,13] However, for intravalley scattering in SiGe it has been shown experimentally that two phonon mode behaviors coexist: Si and Ge modes which are never averaged. Our model assumes that the scattering strengths are proportional to the molar fraction of Ge_x (Ge modes) or $(1-x)$ (Si modes).[24] In SiGe it is essential to consider alloy scattering which is contemplated here based on the model of Harrison and Hauser.[25] In addition, strain affects the relative importance of intra- and intervalley scattering mechanisms due to the changes induced in the band structure.[26]

Having fixed a consistent set of transport parameters, prior to calculation of the static characteristics and noise characteristics of the one-dimensional $Si_{1-x}Ge_x$/Si structures, Monte Carlo simulation was performed for relaxed and strained SiGe to validate the choice of certain parameters of the simulation. Evaluation of silicon low-field mobility for electrons and holes revealed the agreement with experimental and analytical results for impurity densities up to 10^{18} cm^{-3}.[27–29] No systematic mobility investigation on relaxed bulk-like SiGe epilayers has been performed to date. The problems with the fabrication of SiGe with a homogeneous Ge content and controlled doping concentration yield a scattering of experimental data.[14,30] Not only the modification of effective masses and the above described scattering mechanisms but also the inclusion of alloy scattering are essential to explain the experimental data for relaxed SiGe alloys. Different values of the alloy potential, ΔU, have been employed to obtain consistent mobility results in satisfactory agreement with the available experimental information for electron mobility in relaxed alloys[30] and with Monte Carlo simulations for relaxed and strained SiGe.[31] The best fit is obtained with ΔU equal to 0.6 eV for electrons and holes, in reasonable agreement with the most recent values proposed in the literature.[20,32] Our results show that under low doping conditions, on SiGe layers alloy scattering degrades mobility. However, since the impurity concentration increases this ceases to be so. Consequently, certain Ge contents and doping density conditions may compensate the reduction in the charge carrier mobility caused by alloy scattering and raise electron mobility above its Si value.[26,31,33] Our model predicts an increase in hole mobility in strained bulk-like SiGe layers.[34,35] In modern device applications, scaling-down device dimensions can lead to relatively high fields. Under these conditions our simulation confirms a reduction in the strain-induced mobility enhancement.

III. SIMULATED STRUCTURES

The devices considered have the same specifications in regards to geometry and abrupt doping profiles: a 0.3 μm unstrained p^+-type Si region with a doping of 10^{23} m^{-3} and a 0.4 μm n-type region with a doping of 5.0×10^{21} m^{-3}. Two materials were considered for the n region: Si and $Si_{0.7}Ge_{0.3}$, yielding two different structures: a silicon p^+n homojunction ($D1$) and a p^+-Si/n-$Si_{0.7}Ge_{0.3}$ heterojunction ($D2$). In $D2$, the n region is assumed to be uniformly grown with a strained SiGe layer and the leading edge of the Ge profile is the metallurgical pn junction. A Ge content equal to 0.3 is considered so that a substantial band offset and strain effects are ensured. Figure 1 shows the schematic cross section and doping level of the heterojunction. The band alignments for $Si_{0.7}Ge_{0.3}$ grown on Si substrate are also depicted.[14] The band discontinuities at the junction are $\Delta E_c = 30$ meV and $\Delta E_v = 260$ meV for the CB and VB, respectively.[14,36] It is worth comparing the Si and SiGe bands in order to emphasize the relevant features. In Si, the

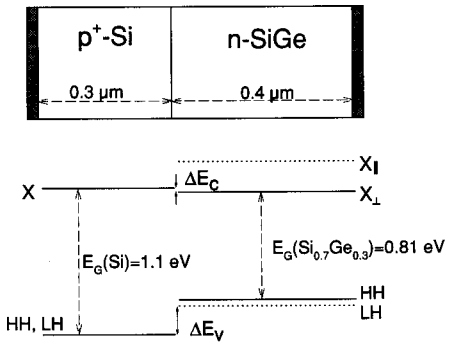

FIG. 1. Scheme of p^+n structures with their characteristic parameters, the fraction of germanium, and the valence and conduction band offsets.

$X_\perp$ and $X_\parallel$ levels are degenerated, yielding the minimum of the CB, and also the HH and LH subbands. The SiGe layer exhibits a lifting of these degeneracies owing to epitaxial strain. Due to the relatively high value of the molar fraction of Ge considered, the $X_\parallel$ level in SiGe lies above the X valley on Si. This strongly affects the transport of electrons at the junction, as discussed below.

Ideal classical transitions and the absence of tunnel current at the spike (this is feasible owing to the modest doping levels) have been assumed.[37] Generation–recombination processes (band–band, band–impurities, etc.) and the effects of degeneracy and scattering by neutral impurities are not included due to the above-mentioned small length and doping profiles of the devices. The most relevant material parameter for pseudomorphic layers is the critical thickness t_c.[38–40] If this thickness increases beyond t_c, strain relaxation of the SiGe alloys becomes energetically favorable. Despite the nonrealistic SiGe strained-layer dimension (0.3 μm) in the heterojunction, we study this structure in order to compare the current-mode noise results of $D2$ with those previously reported for $D1$.[9]

IV. STATIC $J-V$ CHARACTERISTICS

Figure 2 shows the forward total current density (J)-voltage (V_{appl}) characteristics of the above structures, $D1$ and $D2$, and their decomposition into the contributions of holes and electrons. Comparison of J between $D1$ and $D2$ reveals a higher current level in $D2$ for the same bias voltage as a consequence of several factors: band discontinuities, differences in scattering rates, and carrier effective masses between Si and strained $Si_{0.7}Ge_{0.3}$. This phenomenon is consistent with the previously observed experimental[41] results and Monte Carlo simulations.[31] The forward bias range considered in our former analysis of a p^+n homojunction ($D1$) is centered on the homojunction built-in potential, V_{bi}^{D1}. This range was chosen for two main reasons.[9] First, regarding static results, the dependence of J displays a switch from exponential to linear behavior close to this voltage value. Second, V_{bi}^{D1} is an important feature involved in noise characterization because it acts as a reference for limiting the edges of the shot, thermal, and excess noise ranges. These reasons also apply to $D2$ and, therefore, analysis of the heterojunction was also performed for a voltage range around the built-in voltage of this structure (V_{bi}^{D2} close to V_{bi}^{D1}).[42]

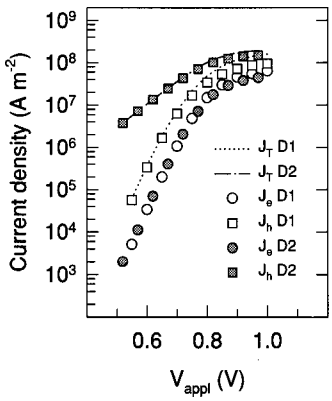

FIG. 2. $J-V$ characteristics of the structures studied. Total current (lines), electron current (circles), and hole current (squares). Homojunction currents are defined by white symbols and the dotted line. Abrupt heterojunction currents are denoted with grey symbols and the dashed–dotted line.

In the case of $D1$, while the applied voltage (V_{appl}) $< V_{\text{bi}}^{D1}$, the electron and hole current densities follow exponential behavior, in agreement with the theoretical model of a short diode.[43] For $V_{\text{appl}} > V_{\text{bi}}^{D1}$, in $D1$ the currents of electrons and holes no longer show exponential behavior and tend to exhibit linear behavior. Moreover, the value of the electron current approaches that of the holes owing to the greater mobility of the former carriers. In view of the $J-V$ characteristics of $D2$ (Fig. 2), within the range considered, two significant differences can be seen with respect to those of $D1$. On the other hand, the hole-electron current ratio is larger than in the homojunction case, reflecting the existence of the remarkable discontinuity at the heterojunction in the VB. On the other hand, the presence of potential spikes modifies the features of the $J-V$ characteristics. For $V_{\text{appl}} < V_{\text{bi}}^{D2}$, the slope of the hole current density characteristic still exhibits an exponential dependence but its slope is different from that predicted by the short diode model whereas the electron current continues to show such a dependence.

Figure 3 shows a comparison of the electron (a) and hole (b) densities through $D1$ and $D2$ for two bias conditions (one included in the exponential range, 0.65 V). The conduction and valence band diagrams for $D1$ and $D2$ along the device for this bias condition are also shown in Figs. 3(a) and 3(b), respectively. The difference in the energy band gaps in $D2$ at the junction and the absence of any energy discontinuities in $D1$ should be noted. In the low doped region of $D1$, for $V_{\text{appl}} = 0.65\ \text{V} < V_{\text{bi}}^{D1}$, the minority carrier density (holes) is lower than that of the majority ones (electrons). The electric field distribution is typical of an ideal p-n junction: it is different from zero throughout the spatial charge region (showing a maximum in absolute value at the metallurgic junction) and is abolished as the ohmic contacts are approached [Fig. 4(a)]. The whole of the potential drop is essentially localized in the spatial charge region of the junction and is reflected in the exponential behavior of the current of both types of carriers (barrier-limited current transport). For $V_{\text{appl}} = 0.85\ \text{V} > V_{\text{bi}}^{D1}$ the barrier becomes negligible and the applied voltage begins to drop along the whole device. Under these conditions the junction behaves as a ''re-

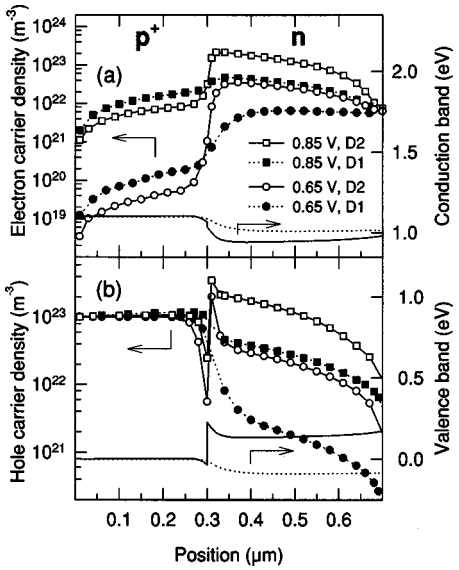

FIG. 3. (a) Comparison of electron concentrations through $D1$ (closed symbols) and $D2$ (open symbols) for 0.65 V (circles) and 0.85 (squares) and the bottom of the conduction band for $D1$ (dotted line) and $D2$ (dashed–dotted line). (b) Comparison of hole concentrations through $D1$ (closed symbols) and $D2$ (open symbols) for 0.65 V (circles) and 0.85 (squares) and the top of the valence band for the Si p^+n homojunction (dotted line) and the $Si/Si_{0.7}Ge_{0.3}$ heterojunction (dashed–dotted line).

sistance,'' varying with the bias. The vanishing of the diffusion barrier forces the n region towards high-injection conditions. The hole concentration in this region becomes larger than the doping profile and hence the majority carrier density must follow the minority one in order to ensure charge quasineutrality (Fig. 3). In these conditions, a noticeable electric field must appear in the quasineutral n region (Fig. 4) and the potential also drops in this region.[43] The particle injection algorithm at the contacts[44] guarantees that

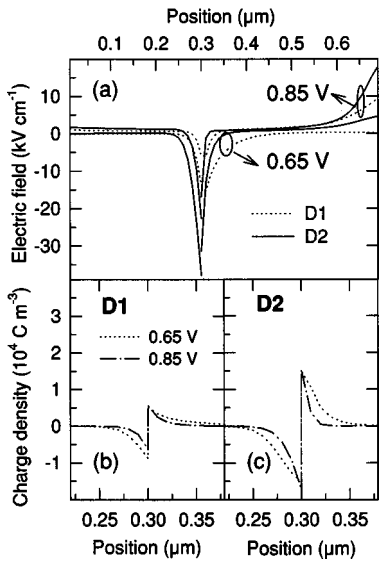

FIG. 4. (a) Average electric field in $D1$ (dotted line) and $D2$ (solid line) for two different values of applied voltage. Evolution with voltage of charge density in the region close to the junctions for the Si p^+n homojunction (b) and the $Si/Si_{0.7}Ge_{0.3}$ heterojunction (c).

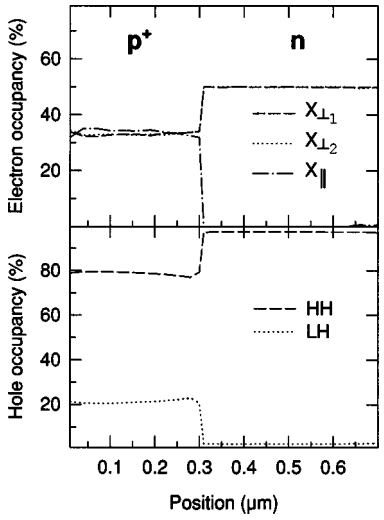

FIG. 5. Relative average band population of different X valleys of the conduction band and heavy and light hole subbands of the valence band through the $Si/Si_{0.7}Ge_{0.3}$ heterojunction and an applied voltage equal to 0.65 V. No meaningful variations are observed with the increase in bias.

the majority carrier density is equal to the doping concentration in order to assure the ohmic character[45] of these contacts.

Deeper analysis of internal magnitude profiles is needed in $D2$ in order to illustrate the influence of both the lifting of degeneracy and the effect of the band discontinuities on the current densities described above. The former factor can readily be analyzed by examining the relative average valley population of the CB valleys and of the VB subbands for a bias condition of 0.65 V through $D2$ (Fig. 5). In the strained SiGe layer, the splitting-up of the $X_\parallel$ valleys explains their weak population (roughly zero). Thus, a significant percentage of the electrons that pass over the barrier into the p^+-Si region must undergo an intervalley scattering in order to guarantee an accurate population in all the X valleys for a weak electric field (not far from equipopulation).[13] In this way, the average conduction mass of the electrons increases when these carriers pass into the silicon region. Regarding the occupancy of the holes, the effect of the strain is severe on the VB. A larger population of the HH band arises in $Si_{0.7}Ge_{0.3}$ with respect to that obtained for the silicon layer. In addition to the phenomena related to the strain, the effect of the band discontinuities on current density must also be examined. In $D2$, in their passage from the n-$Si_{0.7}Ge_{0.3}$ region towards to the p^+-Si region the electrons encounter an important barrier (the one due to diffusion potential but increased by 30 meV) (see Fig. 3), which is reflected in the exponential behavior of the electron current. The injection of electrons from the n region to the p^+ region is therefore strikingly reduced. The effect of the spike (Fig. 3) in the VB means that the transport of holes is favored in comparison with the situation in $D1$. In conclusion, the most significant effect introduced by the interface discontinuity is that of permitting selectivity in the type of carrier that supports the current in the structure.

Figure 3 also shows the differences appearing in the free carrier densities between $D2$ and $D1$ under two identical

bias conditions. First, in $D2$, even for a forward voltage of 0.65 V the presence of the spike in the valence band around the interface yields an excess of electrons in the n region to compensate electrically the strong accumulation of holes (high-injection conditions). Thus, an imbalance already appears between the majority carrier density in the n region and that of ionized impurities owing to the presence of the barrier and leads to a nonnegligible electric field in the n neutral region. The nature of the spatial charge (mobile charge) on the n side of $D2$ yields the dipole charge density at the interface and therefore the interface field being larger in the case of the heterojunction [Figs. 4(a)–4(c)]. At the same time, a still important barrier (mainly for electrons) persists. As a result, the current in the structure is mainly formed of holes and is controlled both by the VB discontinuity and the drop in voltage in the quasineutral region n, such that it does not have a purely exponential character. These different characteristics of the heterojunction with respect to the homojunction have strong repercussions on noise behavior.

V. THEORETICAL ANALYSIS OF CURRENT FLUCTUATIONS

Prior to offering the noise results, it is essential to develop a theoretical analysis that will allow us to calculate, analyze, and compare the noise characteristics of both structures. To investigate current fluctuations in the current–noise operation mode the voltage applied to the electrodes must remain constant and the current must be allowed to fluctuate.[46] The mathematical quantities that characterize the current noise are the autocorrelation function of the total current fluctuations, $C_I(t)$,[9] and the spectral density of the total current fluctuations $S_I(f)$. In a bipolar structure, the total current can be expressed in terms of the contributions of electrons and holes. The complexity of the analysis of $C_I(t)$ and $S_I(f)$ in a bipolar structure can be overcome by expressing these quantities by means the terms associated with the electron and hole current fluctuations $C_{Ie}(t)$ and $C_{Ih}(t)$, respectively, and the cross correlation between electron and hole current fluctuations $C_{Ic}(t)$[25]

$$C_I(t)=\overline{\delta I(0)\,\delta I(t)}=C_{Ie}(t)+C_{Ih}(t)+C_{Ic}(t), \tag{1}$$

$$S_I(f)=2\int_{-\infty}^{\infty} C_I(t)e^{j2\pi ft}dt=S_{Ie}(f)+S_{Ih}(f)+S_{Ic}(f). \tag{2}$$

Comparison of $C_{Ie}(t)$, $C_{Ih}(t)$, $C_{Ic}(t)$ between $D1$ and $D2$ does not always afford straightforward conclusions. In order to clarify the origin of current fluctuations in both structures, and taking into account that they have an identical p^+ region, it is useful to manipulate the calculation of the electron and hole currents. Calculation of the electron current, $I_e(t)$, can be performed by determining as a function of time the number of electrons that remain inside the p^+ and n regions of the devices, $N_{\mathrm{Te}_1}(t)$ and $N_{\mathrm{Te}_2}(t)$, respectively. The electron current is then given by

$$I_e(t)=\frac{q}{L}\sum_{i=1}^{N_{\mathrm{Te}_1}(t)}\nu_i(t)+\frac{q}{L}\sum_{j=1}^{N_{\mathrm{Te}_2}(t)}\nu_j(t)=I_e^{p^+}(t)+I_e^{n}(t). \tag{3}$$

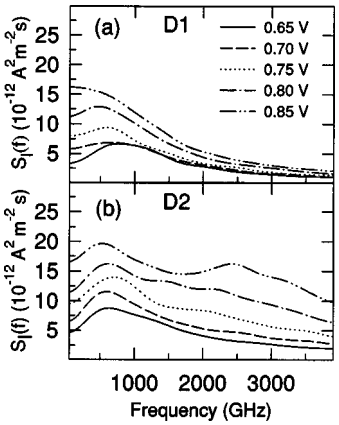

FIG. 6. Spectral density of total current fluctuations as a function of the frequency of the Si p^+n homojunction (a) and the Si/$Si_{0.7}Ge_{0.3}$ heterojunction (b) for different bias conditions. The line types and applied voltages are valid for both plots.

A parallel expression can be written for the hole current, $I_h(t)$.

According to Eq. (1), $C_{Ie}(t)$ can be written:

$$C_{Ie}(t)=C_{Ie}^{p^+p^+}(t)+C_{Ie}^{nn}(t)+C_{Ie}^{p^+n}(t)+C_{Ie}^{np^+}(t), \tag{4}$$

where $C_{Ie}^{p^+p^+}(t)$ and $C_{Ie}^{nn}(t)$ are the autocorrelation functions of current fluctuations of electrons in the p^+ and in the n regions, respectively. $C_{Ie}^{np^+}(t)$ and $C_{Ie}^{p^+n}(t)$ are the terms related to the cross correlation between current fluctuations of electrons in the p^+ and n regions of the device. By analogy with Eq. (4), a similar derivation can be performed for $C_{Ih}(t)$ and $C_{Ic}(t)$.

Moreover, the terms $S_{Ie}^{p^+p^+}(f)$, $S_{Ie}^{nn}(f)$, $S_{Ie}^{np^+}(f)$, and $S_{Ie}^{p^+n}(f)$, which establish the spectral density of electron current fluctuations, $S_{Ie}(f)$, can be determined following an identical treatment as performed for $C_{Ie}(t)$, which gives

$$S_{Ie}(f)=S_{Ie}^{p^+p^+}(f)+S_{Ie}^{nn}(f)+S_{Ie}^{p^+n}(f)+S_{Ie}^{np^+}(f). \tag{5}$$

Equation (2) describes as a function of frequency which type of carrier contributes to the spectral density of current fluctuations in the device. Equation (5) and the analogous derivations performed for $S_{Ih}(t)$ and $S_{Ic}(t)$ can be used to predict in which region of the device, and as a function of frequency, this noise is being originated.

VI. COMPARATIVE STUDY OF CURRENT FLUCTUATIONS IN Si AND Si/SiGE p^+n STRUCTURES

To gain insight into the real meaning of these mathematical quantities, we begin by discussing the noise characteristics for both structures. The spectral density of total current fluctuations, $S_I(f)$, as a function of frequency is plotted in Fig. 6 for the Si p^+n homojunction (a), and Si/$Si_{0.7}Ge_{0.3}$ heterojunction (b), and several bias conditions. A first glance reveals that two different ranges of behavior can be observed in the evolution with a bias of $S_I(f)$ in the heterojunction. In the first range (corresponding to applied voltages up to 0.75 V), the dependence of $S_I(f)$ on bias in $D2$ is qualitatively similar to that occurring in $D1$. That is, $S_I(f)$ exhibits a

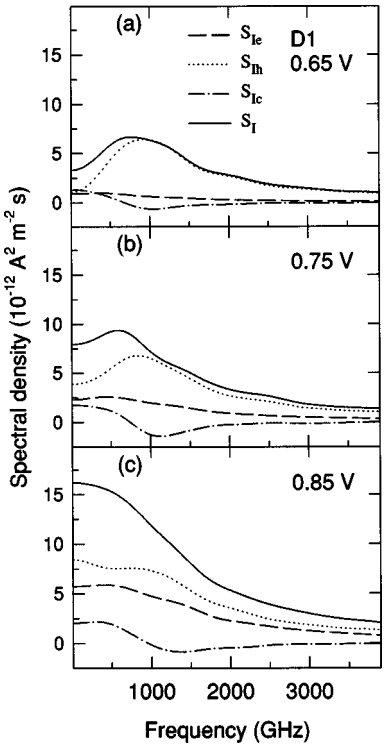

FIG. 7. Decomposition of the spectral density of total current fluctuations in the homojunction for three different bias conditions: 0.65, 0.75, and 0.85 V.

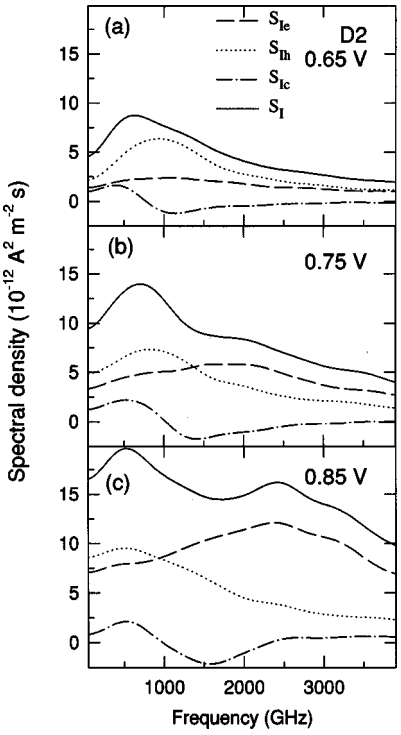

FIG. 8. Decomposition of the spectral density of total current fluctuations in the Si/SiGe heterojunction for the same bias conditions considered in Fig. 7: 0.65, 0.75, and 0.85 V.

single maximum whose frequency is slightly modified as bias increases in a range between 800 and 500 GHz. In $D2$, for voltages beyond 0.75 V, a pronounced peak around 600 GHz is still present in $S_I(f)$. However, two main differences can be seen on comparing the $S_I(f)$ results of $D1$ and $D2$; whereas for $D1$ an increase depending on bias in $S_I(f)$ is restricted to frequencies below 1000 GHz, in $D2$ a remarkable increase in the 2000–2500 GHz range occurs. These differences mean that by placing a SiGe layer in the n region of the device structure, not only the static characteristics are strongly affected but also the presence of germanium implies changes in the noise characteristics, especially in a very high frequency range. Below, an attempt is made to determine precisely how strain and band discontinuities particularly affect current fluctuations and hence directly determine the noise behavior.

We start our detailed analysis with a brief discussion of noise in the homojunction and then extend this to the abrupt heterojunction (for a more detailed discussion see Ref. 9). It should be stressed that current fluctuations can be originated via fluctuations in velocity and/or carrier numbers, although in the present case has been proved that the presence of space-charge effects leads the carrier number fluctuations to be negligible due to screening effects.[47] Thus, $C_{Ie}(t)$, $C_{Ih}(t)$, and $C_{Ic}(t)$ are only determined by the contributions of the autocorrelation function of velocity fluctuations.[8] This contribution is expressed in terms of the mean number of particles and the carrier velocity fluctuations. Therefore, the increase in $C_{Ie}(t)$, $C_{Ih}(t)$, and $C_{Ic}(t)$ would be due to the increase in both the mean carrier number of particles and the velocity fluctuations.[9] In accordance with the approach described in Sec. V, based on the individual analysis of electron and hole contributions to noise, decomposition of $S_I(f)$ into $S_{Ie}(f)$, $S_{Ih}(f)$, and $S_{Ic}(f)$ yields the situation depicted in Figs. 7 and 8 in $D1$ and $D2$, respectively, for three different bias conditions. The main features that characterize noise in $D1$ are shown in Fig. 7 and can be summarized as follows:[9] In the barrier-limited current regime, the value of the spectral density of total current fluctuations at low frequency, $S_I(O)$, displays a shot type noise behavior, which is determined by individual carriers crossing the barrier randomly (dependence proportional to total current, I). The influence of the minority carriers of the high doped region (electrons) only has an effect at low frequencies, not on the maximum of $S_I(f)$. This maximum is associated exclusively with the plasma frequency of holes in the p^+ region, f_{p+}, [Fig. 7(a)]. In the intermediate current range (voltages around V_{bi}^{D1}), $S_I(O)$ tends towards a constant value, independent of I, which arises from the fluctuations in carrier velocity (thermal noise). Hence, as the barrier disappears the higher mobility of electrons renders the electron current comparable to that of the holes (Fig. 2). This reasoning is also applicable when considering noise, and higher electron mobility leads to an increase in the S_{Ie} contribution. Thus, larger fluctuations of electrons in the n region of the device become a strong competitor of hole plasma oscillation in the p^+ region. This increase in S_{Ie} directly determines the shift towards lower frequencies of the $S_I(f)$ maximum, which currently lies around 500 GHz, Fig. 7(b). In the high-injection regime, the presence of hot carriers (holes in the n region) is responsible for excess noise (usually proportional to I^2), leading $S_I(O)$ to increase strongly [Fig. 7(c)].

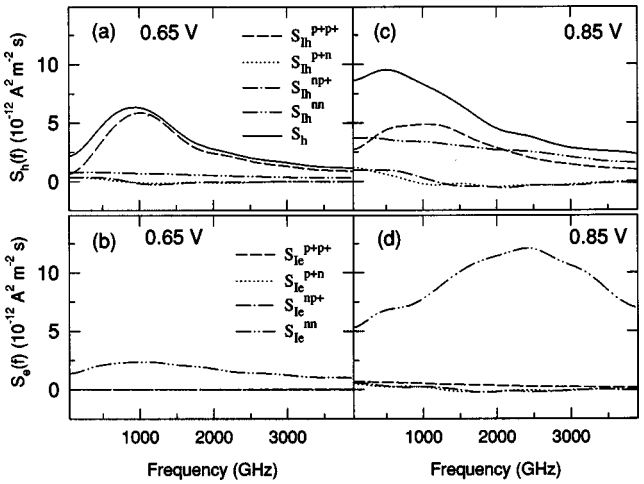

FIG. 9. Spatial decomposition of the spectral density of total current fluctuations of holes and electrons for a weak voltage 0.65 (a) and (b), respectively, and for high-injection conditions, 0.85 V (c) and (d), respectively, in the heterojunction.

For a deep understanding of the differences in noise characteristics between $D1$ and $D2$, mentioned above and based on the physical constraints involved, it is advantageous to examine the results of $D2$ by a parallel procedure to the one employed for $D1$. Even for the weaker bias (0.65 V), a strong accumulation of electrons and holes, not present in $D1$, takes place in the $Si_{0.7}Ge_{0.3}$ region of $D2$, as was discussed in Sec. IV. As can be seen, S_{Ih} exhibits a dependence on frequency in $D2$ [Fig. 8(a)] identical to the behavior found in $D1$ [Fig. 7(a)]. When studying the terms yielding the spatial decomposition of S_{Ih} and S_{Ie} [Figs. 9(a) and 9(b)] two important issues emerge. On one hand, the main contribution of S_{Ih} is linked exclusively to hole current fluctuations in the p^+ region of the device; that is, it shows its maximum located around the plasma frequency of holes in the Si region, f_{p+}. Therefore, a weaker effect is found for the S_{Ih}^{nn} component even though the valence band spike and the pseudomorphic layer prevent the hole current from having a purely exponential character (Fig. 2). On the other hand [Fig. 9(b)], in $D2$ the S_{Ie} component is entirely determined by current fluctuations linked to majority carriers of the n-$Si_{0.7}Ge_{0.3}$ region. In addition, on comparing both structures, the S_{Ie} component is seen to be considerably larger in $D2$. As was discussed in Sec. II, for this low doping concentration the results on low field bulk mobility show no increase in electron mobility in SiGe for a Ge content equal to 0.3. Therefore, the increase in carrier numbers in the n region of $D2$ is the only aspect responsible for the larger electron current fluctuation whereas it causes no effect for this bias conditions on hole fluctuations [Figs. 7(a) and 8(a)].

As may be seen in Fig. 6, upon increasing the bias (0.75 and 0.85 V) in the heterojunction the frequency of the $S_I(f)$ maximum is modified, as occurs in $D1$. In $D1$, while the hole component, S_{Ih}, maintains the maximum at f_{p+}, the bias increase leads the electron component, S_{Ie}, to become more important and forces the shift of the $S_I(f)$ maximum. However, in $D2$ [Figs. 8(b) and 8(c)] the reason for this shift lies essentially in the hole component, and the electron fluctuations are the main agents responsible for the additional maximum of $S_I(f)$ at 2500 GHz. To properly explain the origin of these phenomena occurring at high bias conditions, which yield the most noteworthy differences with respect to the silicon homojunction, it is necessary to perform the spatial decomposition of S_{Ih} and S_{Ie}. This is depicted in Figs. 9(c) and 9(d), corresponding to bias conditions of 0.85 V. It is important to bear in mind that a very high electron and hole carrier concentration is found on the SiGe layer, in which both magnitudes reach values as large as 2×10^{23} cm^{-3} in a small zone of the n region for 0.85 V (Fig. 3). From the spatial analysis of $S_I(f)$, it is clear that even for very high-injection conditions S_{Ie} continues to be supported by electrons from the $Si_{0.7}Ge_{0.3}$ region of the device [Fig. 9(d)]. Owing to the high electron concentration and the low conduction mass of this type of carriers exclusively located in $X_\perp$ valleys in the SiGe region, the maximum S_{Ie} is located at high frequency values (2500 GHz). Regarding the spectral density of the hole current fluctuations, the low significance at very high frequencies of the S_{Ih}^{p+n} and S_{Ih}^{np+} components indicates a lack of coupling of hole current fluctuations between the p^+ and n regions. However, in the high voltage regime, the S_{Ih}^{nn} component plays an essential role in hole noise characteristics, which is combined with the importance for all bias ranges of the standard hole component, S_{Ih}^{p+p+} [Fig. 9(c)]. This increased the importance of S_{Ih}^{nn} originated by the rise in the hole concentration and the enhancement of hole mobility in SiGe leads to the following results. First, S_{Ih}^{nn} acts as a strong support for the shift towards lower frequencies of the maximum of the S_{Ih} component, and therefore the 0–800 GHz maximum of S_I. Additionally, the increase in the low frequency value of S_{Ih}^{nn} is essentially due to the heating of holes in the SiGe region of the heterostructure owing to the nonnegligible electric field (Fig. 4). Second, the S_{Ih} component does not tend monotonously towards zero when frequency increases [Fig. 8(c)], as was observed in $D1$ [Fig. 7(c)], but shows a small almost imperceptible peak around 2500 GHz related to the increase in S_{Ih}^{nn}. This factor is involved in the meaningful increase in $S_I(f)$ at that frequency, in which the main component responsible is S_{Ie}^{nn}. This indicates the onset of an oscillation at 2500 GHz related to strong electron current fluctuations in the $Si_{0.7}Ge_{0.3}$ region slightly coupled with current fluctuations of high mobility holes. This can be checked by examining the cross correlation term between electrons and holes, S_{Ic}, which has been ignored until now. In Figs. 7 and 8 it may be seen how the S_{Ic} component gains importance in the heterojunction. Low frequency analysis of the spectral density of total current fluctuations versus the current density of the heterojunction reveals a nondivergent behavior in comparison to the homojunction: the presence of thermal, shot, and excess noise ranges can be easily observed.

VII. CONCLUSIONS

A detailed study of the physical origin of the high frequency noise phenomena that characterize the characteristics of $Si_{1-x}Ge_x$/Si heterojunctions has been reported. The fea-

tures of our one-dimensional bipolar Monte Carlo simulator are discussed in specific relation to the transport properties of a strained SiGe layer grown on a Si substrate. A theoretical analysis based on a spatial analysis of noise to isolate the influence of both types of carrier in the Si and $Si_{1-x}Ge_x$ epilayers of the devices allows us to calculate and compare the noise characteristics of both structures. Using this method we investigate the combined effects of the germanium profile, band discontinuities, and strain on noise characteristics.

The presence of spikes and discontinuities in the valence and conduction bands, respectively, modifies the features of the $J-V$ characteristics of the heterojunction with respect to those of the homojunction. Thus, hole current largely predominates over electron current. Furthermore, the hole current does not have a purely exponential character because it is controlled both by the remarkable valence band discontinuity and the drop in voltage in the SiGe region *n*, which shows a strong accumulation of both types of carriers within the bias range considered. Accordingly, the SiGe region of the device operates under high-injection conditions.

The main part of the work deals with a comparative microscopic analysis of current fluctuations in homojunction and heterojunctions over a wide range of frequencies. For the lower voltage range, the dependence on frequency of $S_I(f)$ in the heterojunction is qualitatively similar to that occurring in the homojunction. The only remarkable effect at low biases when compared with the homojunction is that carrier accumulation in the SiGe region is the only phenomenon responsible for larger S_{Ie} and no effect can be imputed to the increase in velocity fluctuations. Hole current fluctuations display an analogous nature as compared with that of the homojunction and depend exclusively on the fluctuations of the majority carriers of the high doped region of the device, p^+ (Si), despite the striking modifications observed in the hole current characteristic. Even for very high-injection conditions within the bias range considered, S_{Ie} is only supported by electrons from the $Si_{0.7}Ge_{0.3}$ region of the device, whose number steadily increases with bias. The pronounced accumulation of holes in the *n* region affords the component of hole fluctuations in the SiGe region a meaningful role when voltage increases, and that component becomes comparable to the standard hole component of fluctuations, S_{Ih}^{p+p+}. The shift in the S_I maximum towards lower frequencies (0–800 GHz) indicates hole heating in the SiGe region of the heterostructure owing to the nonnegligible electric field. This is responsible for the significant effect on $S_I(O)$, however the presence of shot, thermal, and excess noise is also confirmed in the heterojunction. No coupling of hole current fluctuations between the p^+ and *n* regions is found. An additional maximum in the spectral density of total current fluctuations is found in the 2000–3000 GHz range, confirming strong current fluctuations of electrons slightly coupled with current fluctuations of high mobility holes in the $Si_{0.7}Ge_{0.3}$ region.

ACKNOWLEDGMENTS

This work was funded through Research Project TIC95-0652 from the CICYT and Research Project SA11/96 from the Consejería de Educación y Cultura de la Junta de Castilla y León.

[1] S. C. Jain and W. Hayes, Semicond. Sci. Technol. **6**, 547 (1991).
[2] A. Gruhle, H. Kibbel, U. Erben, and E. Kasper, Electron. Lett. **29**, 415 (1993).
[3] A. Van de Ziel, *Noise, Source Characterization, Measurement* (Prentice-Hall, Englewood Cliffs, NJ, 1970).
[4] J. M. Hinckley and J. Singh, Phys. Rev. B **51**, 9648 (1995).
[5] J. M. Hinckley and J. Singh, J. Appl. Phys. **80**, 6766 (1996).
[6] L. Varani, L. Reggiani, T. Kuhn, T. Gonzalez, and D. Pardo, IEEE Trans. Electron Devices **41**, 1916 (1994).
[7] T. Gonzalez, D. Pardo, L. Varani, and L. Reggiani, IEEE Trans. Electron Devices **42**, 1991 (1995).
[8] L. Reggiani, T. Kuhn, and L. Varani, Appl. Phys. A: Solids Surf. **54**, 411 (1992).
[9] M. J. Martín, J. E. Velázquez, and D. Pardo, J. Appl. Phys. **79**, 6975 (1996).
[10] M. J. Martín, D. Pardo, and J. E. Velázquez, Phys. Status Solidi B **204**, 462 (1997).
[11] M. J. Martín, D. Pardo, and J. E. Velázquez, *Proceedings of the 27th European Solid-State Device Research Conference*, edited by H. Grumbacher (Editions Frontieres, Paris, 1997), pp. 340–343.
[12] C. Jacoboni and L. Reggiani, Rev. Mod. Phys. **55**, 645 (1983).
[13] M. J. Martín, T. González, J. Velázquez, and D. Pardo, Semicond. Sci. Technol. **8**, 1291 (1993).
[14] R. Braunstein, Phys. Rev. **130**, 869 (1963).
[15] M. Rieger and P. Vogl, Phys. Rev. B **48**, 14276 (1993).
[16] J. F. Nützel, C. M. Engelhardt and G. Abstreiter. E. Kasper, in *Properties of Strained and Relaxed Silicon Germanium, Data Review Series 12*, edited by E. Kasper (INSPEC, London, 1995).
[17] C. G. van de Walle and R. M. Martin, Phys. Rev. B **34**, 5621 (1986).
[18] R. People, IEEE J. Quantum Electron. **22**, 1696 (1986).
[19] G. E. Pikus and G. L. Bir, *Symmetry and Strain-Induced Effects in Semiconductors* (Wiley, New York, 1974).
[20] M. V. Fischetti and S. E. Laux, J. Appl. Phys. **80**, 2234 (1996).
[21] J. F. Morar, P. E. Batson, and J. Tersoff, Phys. Rev. B **47**, 4107 (1993).
[22] For a recent review of experimental offsets, see, C. G. Van de Walle, in *Properties of Strained and Relaxed Silicon Germanium, Data Review Series 12*, edited by E. Kasper (INSPEC, London, 1995).
[23] O. Madelung, *Semiconductors: Group IV Elements and III-V Compounds* (Springer, Berlin, 1991).
[24] J. S. Lannin, Phys. Rev. B **16**, 1510 (1977).
[25] J. W. Harrison and J. R. Hauser, Phys. Rev. B **13**, 5347 (1976); D. K. Ferry, *Semiconductors* (Macmillan, New York, 1991).
[26] L. E. Kay and W.-W. Tang, J. Appl. Phys. **70**, 1483 (1991).
[27] C. Canali, F. Jacoboni, F. Nava, G. Ottaviani, and A. Alberigi-Quaranta, Phys. Rev. B **12**, 2265 (1975).
[28] G. Ottaviani, L. Reggiani, C. Canali, F. Nava, and A. Alberigi-Quaranta, Phys. Rev. B **12**, 3318 (1975).
[29] D. B. M. Klaassen, Solid-State Electron. **35**, 953 (1992).
[30] G. Busch and O. Vogt, Helv. Phys. Acta **33**, 437 (1960).
[31] B. Pejcinovic, L. E. Kay, T.-W. Tang, and D. H. Navon, IEEE Trans. Electron Devices **36**, 2129 (1989).
[32] K. Yeom, J. M. Hinckley, and J. Singh, J. Appl. Phys. **80**, 6773 (1996).
[33] R. Manku and A. Nathan, IEEE Trans. Electron Devices **39**, 2082 (1992).
[34] J. M. Hincley and J. Singh, Phys. Rev. B **41**, 2912 (1990).
[35] T. Manku, J. M. McGregor, A. Mathan, D. J. Roulston, J.-P. Noel, and D. C. Houghton, IEEE Trans. Electron Devices **40**, 1990 (1993).
[36] S. C. Jain, J. Poortmans, S. S. Iyer, J. J. Loferski, J. Nijs, R. Mertens, and R. Van Overstraten, IEEE Trans. Electron Devices **12**, 2338 (1993).
[37] D. T. Hughes, R. A. Abram, and R. W. Kelsall, IEEE Trans. Electron Devices **42**, 201 (1995).
[38] R. People and J. C. Bean, Appl. Phys. Lett. **47**, 322 (1985).
[39] Y. Kohama, Y. Fukuda, and M. Seki, Appl. Phys. Lett. **52**, 380 (1988).

[40] J. H. Van der Merwe, Surf. Sci. **31**, 198 (1972).
[41] C. A. King, J. L. Hoyt, and J. F. Gibbons, IEEE Trans. Electron Devices **36**, 2093 (1989).
[42] S. L. Chuang, *Physics of Optoelectronic Devices* (Wiley, New York, 1995).
[43] S. Tiwari, *Compound Semiconductor Device Physics* (Academic, New York, 1992).
[44] T. González and D. Pardo, Solid-State Electron. **39**, 555 (1996).
[45] C. Jacoboni and P. Lugli, *The Monte Carlo Method for Semiconductor Device Simulation* (Springer, Wien, 1989).
[46] T. González, D. Pardo, L. Varani, and L. Reggiani, Appl. Phys. Lett. **63**, 3040 (1993).
[47] L. Varani, T. Kuhn, L. Reggiani, and Y. Perlês, Solid-State Electron. **36**, 251 (1993).